Using LDPC-Coded Modulation and Coherent Detection for Ultra Highspeed Optical Transmission

Ivan B. Djordjevic, Milorad Cvijetic, Lei Xu, and Ting Wang

***Abstract*—We propose the coded modulation schemes for ultrahigh-speed transmission (100 Gb/s and above) by using commercially available components operating at 40 gigasymbols/s. The bit-interleaved coded modulation in combination with the low-density parity-check codes that are used as component codes has been applied. The modulation is based on either M-ary quadrature-amplitude modulation or M-ary phase-shift keying. $\mathrm{Log}_2 M$ bits are mapped into the corresponding signal constellation point using either Gray or natural mapping. The coherent detection scheme has been found to outperform the direct detection one and to provide an additional margin much needed for longer transmission distances or for application in an all-optical network scenario.**

***Index Terms*—Bit-interleaved coded modulation (BICM), coherent detection, low-density parity-check (LDPC) codes, optical communications.**

I. Introduction

THE FUTURE Internet traffic growth will need the deployment of optical transmission systems with bit rates higher than the rate of currently available 40-Gb/s systems, as analyzed recently [1]–[7]. However, at those data rates, such as 100 Gb/s and beyond, the signal quality is significantly degraded mainly due to the impact of polarization-mode dispersion (PMD) and intrachannel nonlinear effects. Currently, the main components related to electrically time-division multiplexed (ETDM) transceivers operating at ~100 Gb/s are becoming commercially available, but they are still expensive. On the other hand, there is an option to use commercially available components operating at lower speed as an alternative approach to ultrahigh-speed optical transmission (100 Gb/s and beyond).

In this paper, we present and analyze such a transmission scenario by using commercially available components operating at lower bit rates. The main element in our approach includes the bit-interleaved coded modulation (BICM) scheme (presented in Section II) combined with the low-density parity-check (LDPC) codes used as component codes [1]. In our approach, modulation, coding, and multiplexing are performed in an unified fashion, which means that not only transmission but also all signal processing related to detection and decoding are effectively done at much lower symbol rates (e.g., 40 gigasymbols/s). Accordingly, dealing with the nonlinear effects and PMD becomes more manageable, while the aggregate data rate is maintained at or above 100 Gb/s.

This coding and modulation scheme is combined with coherent detection to gain an additional improvement. We applied the extrinsic information transfer (EXIT) chart analysis to study the convergence behavior. The modulation formats that have been studied in this paper are M-ary quadrature-amplitude modulation (QAM) and M-ary phase-shift keying (PSK), where $M = 2, \ldots, 16$, both combined with either Gray or natural mapping rule. It is worth mentioning that the results presented in our previous work [3], which was related to differential PSK (DPSK) modulation and direct detection scheme, can be considered as a reference case for the comprehensive transmission architecture presented here.

This paper is organized as follows: The bit-interleaved LDPC-coded modulation (BI-LDPC-CM) scheme with coherent detection is introduced in Section II. The iterative demapping and decoding is described in Section III, while the LDPC codes suitable for BICM are introduced in Section IV. Numerical results are reported in Section V, while the most important conclusions are presented in Section VI.

II. BI-LDPC-CM With Coherent Detection

Let us introduce the transmitter architecture employing the BI-LDPC-CM scheme in combination with the coherent detection scheme. It should be mentioned that in this paper, we also analyzed direct detection and used that as a reference case [see Fig. 1(a)–(c)]. The source bit streams coming from m information sources (e.g., carrying 40 Gb/s traffic) are encoded by using identical (n, k) LDPC codes of code rate $r = k/n$ (where k is the number of information bits, and n is the code word length). The LDPC decoder outputs are written to the $m \times n$ block interleaver row-wise. The mapper accepts m bits $c = (c_1, c_2, \ldots, c_m)$ at time instance i from the $(m \times n)$ interleaver column-wise and determines the corresponding M-ary $(M = 2^m)$ constellation point $s_i = (I_i, Q_i) = |s_i| \exp(j\phi_i)$ [see Fig. 1(a)]. In the coherent detection case, the data

Manuscript received May 3, 2007; revised July 18, 2007. This work was supported in part by the National Science Foundation (NSF) under Grant IHCS 0725405 and by NEC Laboratories America.

I. B. Djordjevic is with the Department of Electrical and Computer Engineering, University of Arizona, Tucson, AZ 85721 USA (e-mail: ivan@ece.arizona.edu).

M. Cvijetic is with NEC Corporation of America, Herndon, VA 20171 USA (e-mail: Milorad.Cvijetic@necam.com).

L. Xu and T. Wang are with NEC Laboratories America, Princeton, NJ 08540 USA.

Color versions of one or more of the figures in this paper are available online at http://ieeexplore.ieee.org.

Digital Object Identifier 10.1109/JLT.2007.906791

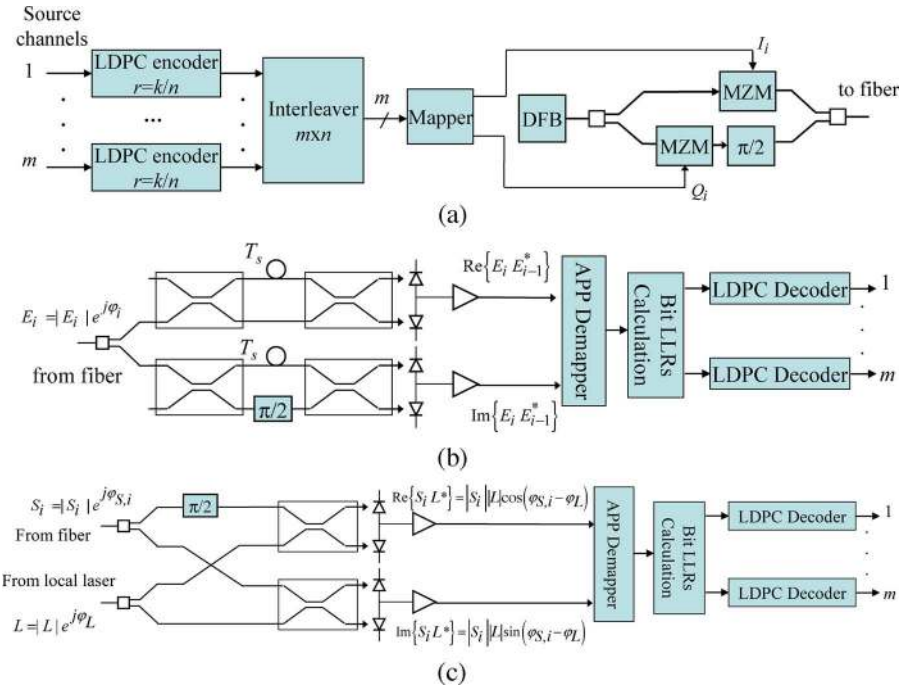

Fig. 1. BI-LDPC-CM scheme. (a) Transmitter architecture. (b) Direct detection as a reference case in accordance to [3]. (c) Coherent detection receiver architecture. $T_s = 1/R_s$, where R_s is the symbol rate.

phasor $\phi_i \in \{0, 2\pi/M, \ldots, 2\pi(M-1)/M\}$ is sent at each ith transmission interval. On the other side, in direct detection, which serves here as a reference case, the differential encoding is required so that the data phasor $\phi_i = \phi_{i-1} + \Delta\phi_i$, where $\Delta\phi_i \in \{0, 2\pi/M, \ldots, 2\pi(M-1)/M\}$ is sent instead at each ith transmission interval. The mapper outputs for M-ary PSK/DPSK I_i and Q_i are proportional to $\cos\phi_i$ and $\sin\phi_i$, respectively. The corresponding signal constellation diagram for 8-PSK/DPSK is given in our recent paper [4]. The coordinates of the ith signal constellation point for a square M-ary QAM signal constellation are given by the equation shown at the bottom of the page. For example, for $M = 16$, the signal constellation points are given by

$$\{I_i, Q_i\} = \begin{bmatrix} (-3,3) & (-1,3) & (1,3) & (3,3) \\ (-3,1) & (-1,1) & (1,1) & (3,1) \\ (-3,-1) & (-1,-1) & (1,-1) & (3,-1) \\ (-3,-3) & (-1,-3) & (1,-3) & (3,-3) \end{bmatrix}.$$

The signal constellation diagrams for different values of M are given in [17].

The receiver input electrical field at time instance i for an optical M-ary DPSK receiver configuration from Fig. 1(b) is denoted by $E_i = |E_i| \exp(j\varphi_i)$. The outputs of the I- and Q-branches [upper and lower branches in Fig. 1(b)] are proportional to $\mathrm{Re}\{E_i E_{i-1}^*\}$ and $\mathrm{Im}\{E_i E_{i-1}^*\}$, respectively. The corresponding coherent detector receiver architecture is shown in Fig. 1(c), where $S_i = |S| e^{j\varphi_{S,i}} (\varphi_{S,i} = \omega_S t + \varphi_i + \varphi_{S,\mathrm{PN}})$ is the coherent receiver input electrical field at time instance i, while $L = |L| e^{j\varphi_L} (\varphi_L = \omega_L t + \varphi_{L,\mathrm{PN}})$ is the local laser electrical field. For homodyne detection, the frequency of the local laser (ω_L) is the same as that of the incoming optical signal (ω_L) so that the balanced outputs of the I- and Q-channel branches [upper and lower branches of Fig. 1(c)] can be written as

$$\begin{aligned} v_I(t) &= R|S_k||L| \cos(\varphi_i + \varphi_{S,\mathrm{PN}} - \varphi_{L,\mathrm{PN}}), \\ &\quad (i-1)T_s \le t < iT_s \\ v_Q(t) &= R|S_k||L| \sin(\varphi_i + \varphi_{S,\mathrm{PN}} - \varphi_{L,\mathrm{PN}}), \\ &\quad (i-1)T_s \le t < iT_s \end{aligned} \tag{1}$$

where R is the photodiode responsivity, while $\varphi_{S,\mathrm{PN}}$ and $\varphi_{L,\mathrm{PN}}$ represent the laser phase noise of the transmitting and receiving (local) laser, respectively. These two noise sources are commonly modeled as a Wiener–Lévy process [8], which is a zero-mean Gaussian process with variance $2\pi(\Delta\nu_S + \Delta\nu_L)|t|$, where $\Delta\nu_S$ and $\Delta\nu_L$ are the laser linewidths of the transmitting and receiving laser, respectively. The transmitted signal constellation point $s_i = |s_i| \exp(j\phi_i)$ can be perfectly

$$\{I_i, Q_i\} = \begin{bmatrix} (-\sqrt{M}+1, \sqrt{M}-1) & (-\sqrt{M}+3, \sqrt{M}-1) & \ldots & (\sqrt{M}-1, \sqrt{M}-1) \\ (-\sqrt{M}+1, \sqrt{M}-3) & (-\sqrt{M}+3, \sqrt{M}-3) & \ldots & (\sqrt{M}-1, \sqrt{M}-3) \\ \vdots & \vdots & \vdots & \vdots \\ (-\sqrt{M}+1, -\sqrt{M}+1) & (-\sqrt{M}+3, -\sqrt{M}+1) & \ldots & (\sqrt{M}-1, -\sqrt{M}+1) \end{bmatrix}$$

recovered in accordance with (1) only in the absence of laser phase noise.

III. Iterative Demapping and Decoding

The outputs at the I- and Q-branches (in either coherent or direct detection case) are sampled at the symbol rate, while the symbol log-likelihood ratios (LLRs) are calculated in *a posteriori* probability (APP) demapper block as

$$\lambda(\boldsymbol{s}) = \log \frac{P(\boldsymbol{s} = \boldsymbol{s}_0|\boldsymbol{r})}{P(\boldsymbol{s} \neq \boldsymbol{s}_0|\boldsymbol{r})} \tag{2}$$

where $P(\boldsymbol{s}|\boldsymbol{r})$ is determined by using Bayes' rule as

$$P(\boldsymbol{s}|\boldsymbol{r}) = \frac{P(\boldsymbol{r}|\boldsymbol{s})P(\boldsymbol{s})}{\sum_{\boldsymbol{s}'} P(\boldsymbol{r}|\boldsymbol{s}')P(\boldsymbol{s}')}. \tag{3}$$

Note that $\boldsymbol{s} = (I_i, Q_i)$ (as mentioned earlier) is the transmitted signal constellation point at time instance i, while $\boldsymbol{r} = (r_I, r_Q)$, $r_I = v_I(t = iT_s)$, and $r_Q = v_Q(t = iT_s)$ are the samples of the I- and Q-detection branches from Fig. 1(b) and (c). $P(\boldsymbol{r}|\boldsymbol{s})$ from (3) is estimated by evaluation of the histograms, i.e., employing a sufficiently long training sequence in a fashion similar to that reported in [1]. We denoted the *a priori* probability of symbol $\boldsymbol{s}$ with $P(\boldsymbol{s})$, while $\boldsymbol{s}_0$ is a referent symbol. We also need to mention that the normalization in (2) is introduced to equalize the denominator from (3). The bit LLRs $c_j (j = 1, 2, \ldots, m)$ are determined from the symbol LLRs of (2) as

$$L(\hat{c}_j) = \log \frac{\sum_{\boldsymbol{s}:c_j=0} \exp\left[\lambda(\boldsymbol{s})\right]}{\sum_{\boldsymbol{s}:c_j=1} \exp[\lambda(\boldsymbol{s})]}. \tag{4}$$

The APP demapper extrinsic LLRs (the difference of demapper bit LLRs and LDPC decoder LLRs from the previous step) for the LDPC decoders become

$$L_{M,e}(\hat{c}_j) = L(\hat{c}_j) - L_{D,e}(c_j). \tag{5}$$

We denoted the LDPC decoder extrinsic LLRs with $L_{D,e}(c)$, which is initially set to zero value. The LDPC decoder is implemented by employing the sum–product algorithm. The LDPC decoder extrinsic LLRs (the difference between the LDPC decoder output and the input LLRs) $L_{D,e}$ are forwarded to the APP demapper as *a priori* bit LLRs $(L_{M,a})$ so that the symbol *a priori* LLRs are calculated as

$$\lambda_a(\boldsymbol{s}) = \log P(\boldsymbol{s}) = \sum_{j=0}^{m-1} (1 - c_j) L_{D,e}(c_j). \tag{6}$$

By substituting (6) into (3) and then (2), we are able to calculate the symbol LLRs for the subsequent iteration. The iteration between the APP demapper and the LDPC decoder is performed until the maximum number of iterations is reached or the valid code words are obtained.

For convergence behavior analysis, the EXIT chart analysis should be performed. To determine the mutual information (MI) transfer characteristics of the demapper, we model the *a priori* input LLR $L_{M,a}$ as a conditional Gaussian random variable [10]. The MI between c and $L_{M,a}$ is determined numerically, as explained in [10]–[12]. Similarly, the MI $I_{LM,e}$ between c and $L_{M,e}$ is numerically calculated but with the probability density function of c and $L_{M,e}$ determined from the histogram obtained by Monte Carlo simulation, as explained in [10]. By observing $I_{LM,e}$ as a function of the MI of $I_{LM,a}$ and the optical signal-to-noise ratio (OSNR, in decibels), the demapper EXIT characteristic (denoted as T_M) is given by

$$I_{LM,e} = T_M(I_{LM,a}, \text{OSNR}). \tag{7}$$

The EXIT characteristic of the LDPC decoder (denoted as T_D) is defined in a similar fashion as

$$I_{LD,e} = T_D(I_{LD,a}). \tag{8}$$

The "turbo" demapping-based receiver operates by passing extrinsic LLRs between the demapper and the LDPC decoder. The iterative process starts with an initial demapping in which $L_{M,a}$ is set to zero, and as a consequence, $I_{LM,a}$ becomes zero as well. The demapper output LLRs described by

$$I_{LM,e} = I_{LD,a} \tag{9}$$

are fed to the LDPC decoder. The LDPC decoder output LLRs described by

$$I_{LD,e} = I_{LM,a} \tag{10}$$

are fed to the APP demapper. The iterative procedure is repeated until the convergence or the maximum number of iterations has been reached. This procedure is illustrated in Fig. 2, where the APP demapper and LDPC decoder EXIT charts are shown together on the same graph. Three modulation formats (8-PSK, 16-PSK, and 16-QAM) are observed, as well as the following mappings: natural, Gray, and anti-Gray. The EXIT curves have different slopes for different mappings. The existence of a "tunnel" between the corresponding demapping and decoder curves indicates that the iteration between demapper and decoder will be successful. The smallest OSNR, at which the iterative scheme starts to converge, is known as the threshold (pinch-off) limit [10]. The threshold limit in the case of 16-PSK [Fig. 2(b)] is about 3 dB worse, as compared to 8-PSK [Fig. 2(a)]. The 16-QAM mapping curve is well above the 16-PSK curve [see Fig. 2(b)], which indicates that the 16-QAM scheme is going to significantly outperform the 16-PSK one.

IV. LDPC Codes

In this section, we will introduce three classes of LDPC codes that are suitable for use in BICM. The first one is the class of girth-8 *regular* LDPC codes, which are structured based on the concept of *balanced-incomplete block designs* (BIBDs) [13]. The second class of codes is that of *irregular* girth-8 LDPC codes obtained from combinatorial objects known as *pairwise balanced designs* (PBDs) [13]. A PBD,

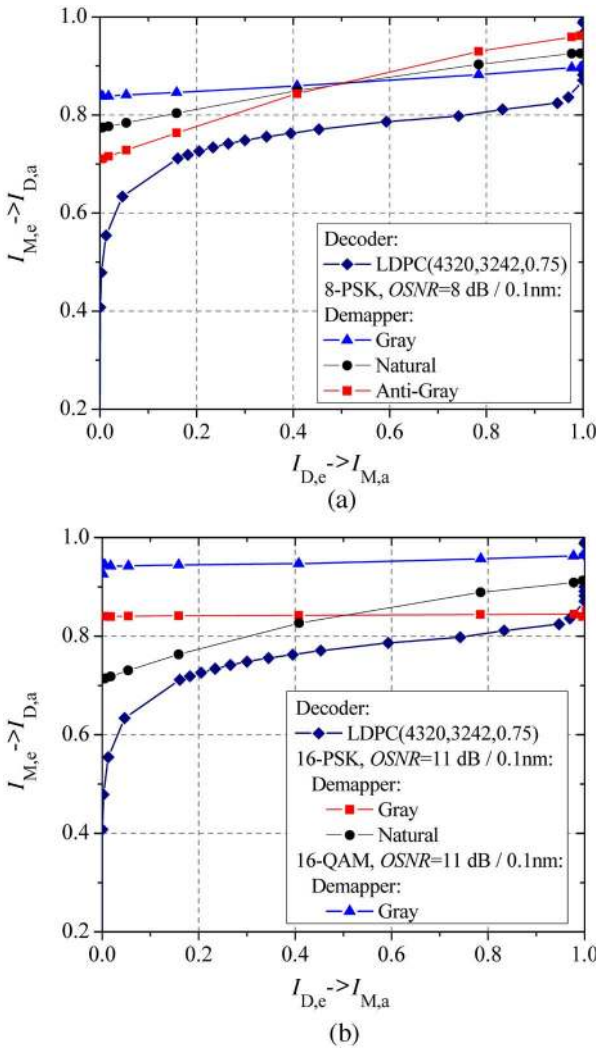

Fig. 2. EXIT chart for different mappings and modulations.

which is denoted as PBD$(v, K, \{0, 1, \ldots, \lambda\})$, is a collection of subsets (blocks) of a v-set V with the size of each block $k_i \in K (k_i \leq v)$ so that each pair of elements occurs in at most λ of the blocks. It should be noticed that we have relaxed the constraint in the definition of PBD from [13] by replacing the word *exact* with *at most*. The purpose of this relaxation is to increase the number of possible PBDs that results in LDPC codes of high code rates. As an example, the blocks $\{1, 6, 9\}$, $\{2, 7, 10\}$, $\{3, 8, 11\}$, $\{4, 12\}$, $\{5, 13\}$, $\{1, 7, 11\}$, $\{2, 8, 12\}$, $\{3, 13\}$, $\{1, 8, 13\}$, $\{2, 9\}$, $\{3, 10\}$, $\{4, 6, 11\}$, $\{5, 7, 12\}$, $\{1, 10\}$, $\{2, 11\}$, $\{3, 6, 12\}$, $\{4, 7, 13\}$, $\{5, 8, 9\}$, $\{1, 12\}$, $\{2, 6, 13\}$, $\{3, 7, 9\}$, $\{4, 8, 10\}$, and $\{5, 11\}$ create PBD$(13, \{2, 3\}, \{0, 1\})$. There are nine blocks of size 2 and 14 blocks of size 3, all with the parameter $\lambda \leq 1$. By considering the elements of blocks as the position of the ones in the corresponding element-block incidence matrix, a parity-check matrix of an equivalent *irregular* LDPC code of girth-6 is obtained. To increase the girth to 8, certain blocks from PBD are to be removed. (The BIBD is a special class of PBD in which all of the blocks are of the same size.)

The third class of codes is the class of block-circulant (BC) LDPC codes [14], which are also known as array LDPC codes

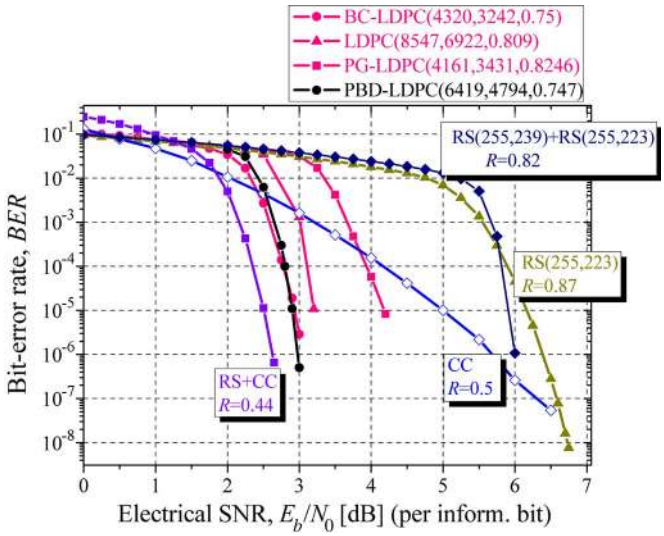

Fig. 3. Performance of the proposed LDPC codes versus performance of PG, RS, convolutional, concatenated RS, and concatenation of convolutional and RS codes on an AWGN channel.

[15] of girth-8. The parity-check matrix of BC codes can be described as

$$\boldsymbol{H} = \begin{bmatrix} P^{i_1} & P^{i_2} & P^{i_3} & \cdots & P^{i_q} \\ P^{i_q} & P^{i_1} & P^{i_2} & \cdots & P^{i_{q-1}} \\ \vdots & \vdots & \vdots & \vdots & \vdots \\ P^{i_{q-r+2}} & P^{i_{q-r+3}} & P^{i_{q-r+4}} & \cdots & P^{i_{q-r+1}} \end{bmatrix} \tag{11}$$

where P is the permutation matrix $P = (p_{ij})_{n \times n}$, $p_{i,i+1} = p_{n,1} = 1$ (zero otherwise). The exponents $i_1, i_2, \ldots, i_q$ in (11) are carefully chosen to avoid cycles of length six in the corresponding bipartite graph of a parity-check matrix. For more details on BC codes, the interested reader is referred to [14].

The proposed LDPC codes are compared against the Reed–Solomon (RS) (255, 223) code, concatenated RS code of rate 0.82, convolutional code (CC) (of constraint length 5), and projective geometry (PG) girth-6 LDPC code (4161, 3431), and the results are shown in Fig. 3. It can be seen that LDPC codes, both regular and irregular, offer much better performance than the other codes. It should be noticed that the PBD-based irregular LDPC code of rate 0.75 is only 0.4 dB away from the concatenation of convolutional RS codes (denoted in the figure as RS + CC) with significantly lower code rate $R = 0.44$ at a bit error rate (BER) of 10^{-6}. As expected, irregular LDPC codes (black colored curves) outperform regular LDPC codes (pink colored curves).

V. Performance Analysis

The results of simulations for 30 iterations in the sum–product algorithm and ten APP demapper–LDPC decoder iterations for an additive white Gaussian noise (AWGN) channel model are shown in Fig. 4 and Table I. The information symbol rate is set to 40 gigasymbols/s, while 8-PSK is employed, so the aggregate bit rate becomes 120 Gb/s. Two different mappers are considered: Gray and natural mapping. The coding gain for 8-PSK at a BER of 10^{-9} is about 9.5 dB, and a much larger coding gain is expected at a BER below 10^{-12}.

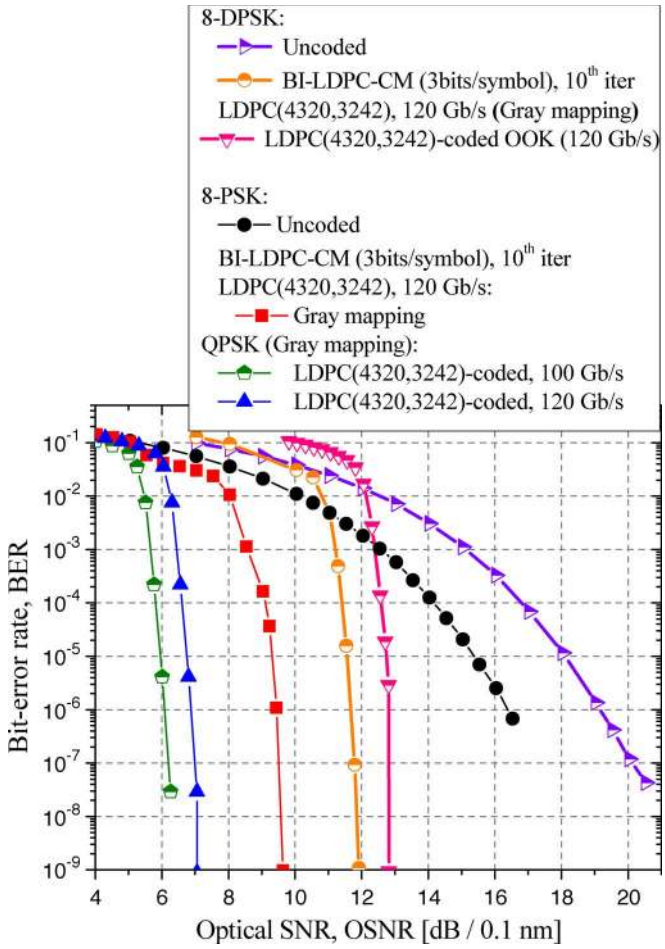

Fig. 4. BER of the coherent detection BI-LDPC-CM scheme versus the direct detection one on an AWGN channel model.

TABLE I
CODING GAIN IMPROVEMENT OVER THE LDPC-CODED ON–OFF KEYING AT A BER OF 10^{-9} FOR AN AGGREGATE RATE OF 120 Gb/s

LDPC(4320,3242)-coded modulation scheme	Coding gain improvement
8-DPSK	0.94 dB
8-PSK	3.23 dB
QPSK	5.23 dB

The coherent detection scheme offers an improvement of at least 2.3 dB, as compared to the corresponding direct detection scheme. The BER performance of the coherent BICM with the LDPC (4320, 3242) code employed as the component code for different modulations is shown in Fig. 5. We can see that 16-QAM (with an aggregate rate of 160 Gb/s) outperforms 16-PSK by more than 3 dB. It is also interesting that 16-QAM slightly outperforms the 8-PSK scheme of lower aggregate data rate (120 Gb/s). The 8-PSK scheme of aggregate rate of 120 Gb/s outperforms the BPSK scheme of data rate 120 Gb/s. Moreover, since the transmission symbol rate for 8-PSK is 53.4 gigasymbols/s, the impact of PMD and intrachannel nonlinearities is much less important than that at 120 G/s. Consequently, for 100-Gb/s Ethernet transmission, it is better to multiplex two 50-Gb/s channels than four 25-Gb/s channels.

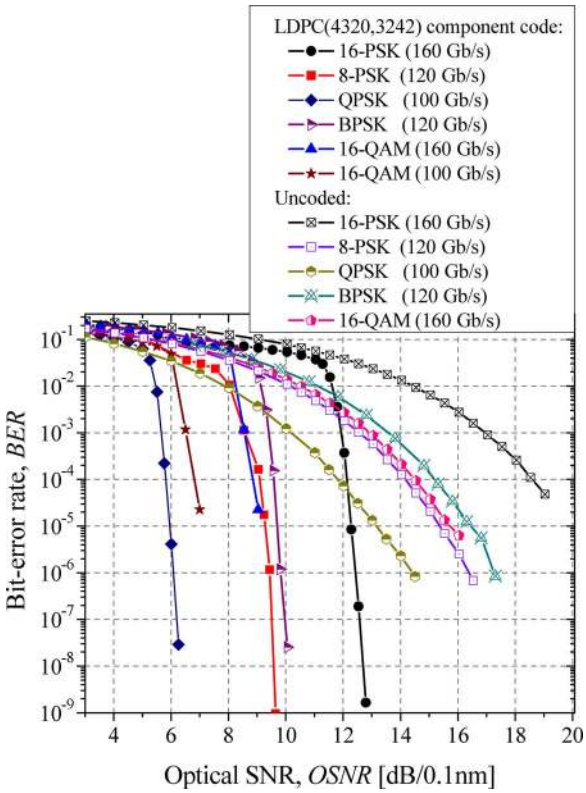

Fig. 5. Performance comparison for different modulation schemes (Gray mapping rule is applied).

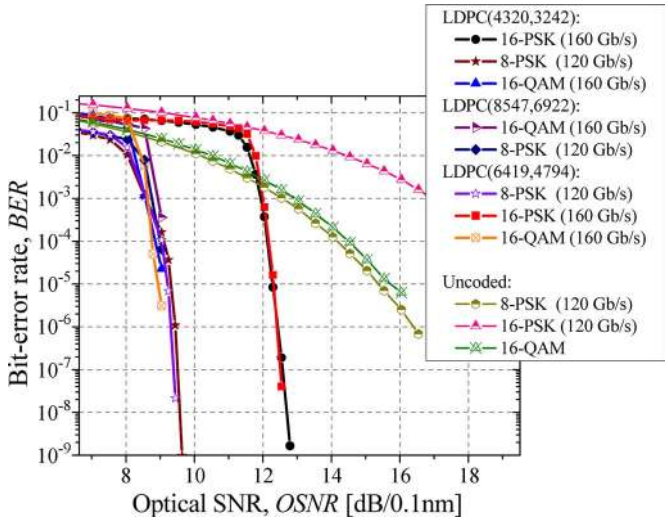

Fig. 6. Comparison for different component LDPC codes (Gray mapping rule is applied).

The comparison for different LDPC component codes is given in Fig. 6. The BICM scheme employing the BIBD-based girth-8 LDPC code of rate 0.81 performs slightly worse or comparable to the BC-based scheme of lower code rate ($R = 0.75$). The BICM scheme of rate 0.75, based on the PBD irregular LDPC code, outperforms the schemes based on regular LDPC codes.

The results of Monte Carlo simulations for the dispersion map shown in Fig. 7 are shown in Fig. 8. The dispersion map under consideration has N spans of total length $L = 120$ km,

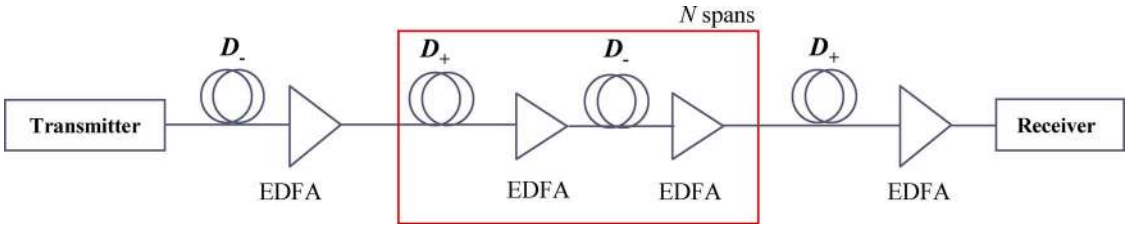

Fig. 7. Dispersion map used for simulations.

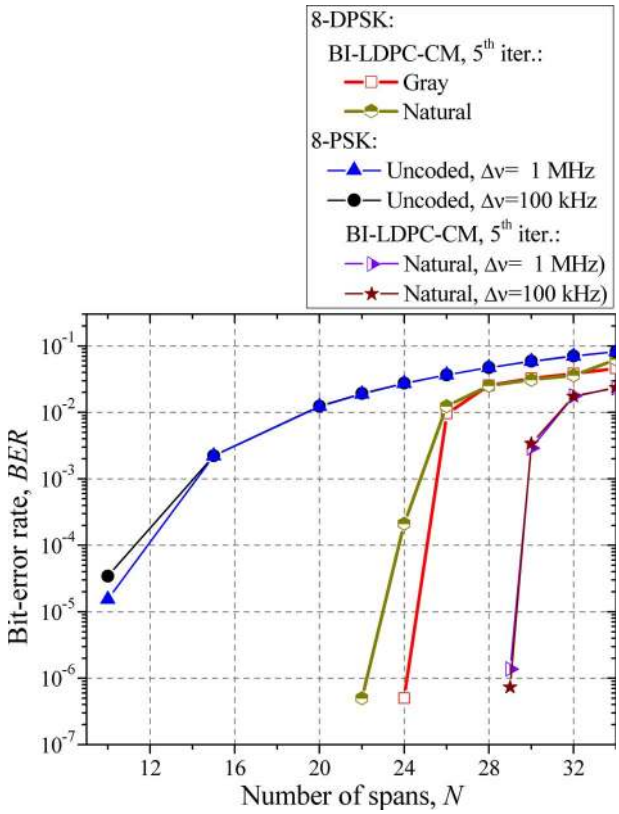

Fig. 8. BER performance of BI-LDPC-CM/coherent detection scheme for dispersion map from Fig. 7.

where each span consists of $2L/3$ km of D_+ fiber followed by $L/3$ km of D_- fiber. The precompensation of -1600 ps/nm is also employed. The fiber parameters are listed in Table II. The simulations were carried out with an average transmitted power per symbol of 0 dBm, and the central wavelength is set to 1552.524 nm, while 8-DPSK/8-PSK with return-to-zero pulses of duty cycle 33% are considered. The propagation of a signal is modeled by the nonlinear Schrödinger equation. The effects of self-phase modulation, nonlinear phase noise, intrachannel cross-phase modulation, intrachannel four-wave mixing, stimulated Raman scattering, chromatic dispersion, laser phase noise, amplified spontaneous emission (ASE) noise, and intersymbol interference are all taken into account. While, by using BI-LDPC-CM and direct detection in a point-to-point transmission scenario, it was possible to achieve the transmission distance of 2760 km at 120-Gb/s aggregate rate with LDPC codes with BER threshold of 10^{-2}, the coherent detection scheme is able to extend the transmission distance by about 600 km. It was shown that the laser phase noise did not have a major impact on transmission performance.

TABLE II
FIBER PARAMETERS

Parameters	D_+ FIBER	D_- FIBER
Dispersion [ps/(nm km)]	20	-40
Dispersion Slope [ps/(nm^{2}km)]	0.06	-0.12
Effective Cross-sectional Area [μm^2]	110	50
Nonlinear refractive index [m^2/W]	$2.6\cdot10^{-20}$	$2.6\cdot10^{-20}$
Attenuation Coefficient [dB/km]	0.19	0.25

To estimate the probability density functions required for the calculation of symbol LLRs [see (2)], we propagated the encoded sequence of length 2^{15} many times for different ASE noise realizations. For more details about this procedure, the interested reader is referred to our recent paper [1].

It was found that the coherent detection for an aggregate rate of 120 Gb/s outperforms the corresponding direct detection scheme by achieving an additional margin of at least 2.3 dB at a BER of 10^{-9}. At the same time, the coherent scheme with an aggregate rate of 160 Gb/s provides 3.2-dB improvement over the direct detection one. With this, we confirm that the advantage increases in proportion to the growth of signal constellation size. It is also worth to notice that 16-QAM provides improvement over 16-PSK in the range of about 3 dB, which was expected having in mind the EXIT charts from Fig. 2(b).

The improvement brought by the coherent detection scheme applied here is very significant from the optical networking perspective if we consider transmission in an all-optical environment where a number of reconfigurable optical add–drop multiplexers (ROADM) and/or wavelength crossconnects (WXC) may be employed at the wavelength path. We assume that the additional margin created by the employment of the coherent detection scheme is enough to keep the same distance as the one attributed to the direct detection scheme in a point-to-point transmission scenario but, this time, with the inclusion of all-optical networking constraints, i.e., penalties due to the deployment of ROADMs and WXC.

Notice that in the simulations above, we assumed that the PMD is compensated by using the LDPC-coded turbo equalization scheme we reported in [16]; therefore, the influence of PMD is not considered here.

VI. CONCLUSION

An ultrahigh-speed transmission architecture, which employs a bandwidth-efficient LDPC-coded modulation, BI-LDPC-CM, and coherent detection scheme, has been proposed. In this architecture, the aggregate bit rate at or above

100 Gb/s is maintained, while modulation, coding, signal processing, and transmission are done at 40 Gb/s, which makes the implementation easier, while the impact of nonlinearities and PMD is less important. From the standardization perspective, and as per International Telecommunication Union Telecommunication Standardization nomenclature, everything is based on the optical data unit (ODU-3) and optical transmission unit (OTU-3), while future ODU/OUT-x $(x > 3)$ are effectively supported. Moreover, once the ETDM technology at 100 Gb/s becomes mature enough, the schemes considered in this paper can be used to achieve transmission at much higher rates than 100 Gb/s. It was also found that the coherent detection scheme is well aligned with the proposed architecture and brings an additional benefit of at least 2.3 dB in power margin at a BER of 10^{-9}, which can be effectively used either to extend the transmission distance by about 25% or to compensate for penalties due to the deployment of ROADMs and WXC. However, this study is left for future research.

REFERENCES

[1] I. B. Djordjevic *et al.*, "Low-density parity-check codes for 40 Gb/s optical transmission systems," *IEEE J. Sel. Top. Quantum Electron.*, vol. 12, no. 4, pp. 555–562, Jul./Aug. 2006.

[2] I. B. Djordjevic and B. Vasic, "100 Gb/s transmission using orthogonal frequency-division multiplexing," *IEEE Photon. Technol. Lett.*, vol. 18, no. 15, pp. 1576–1578, Aug. 2006.

[3] I. B. Djordjevic, M. Cvijetic, L. Xu, and T. Wang, "Proposal for beyond 100 Gb/s optical transmission based on bit-interleaved LDPC-coded modulation," *IEEE Photon. Technol. Lett.*, vol. 19, no. 12, pp. 874–876, Jun. 15, 2007.

[4] I. B. Djordjevic and B. Vasic, "Multilevel coding in *M*-ary DPSK/differential QAM high-speed optical transmission with direct detection," *J. Lightw. Technol.*, vol. 24, no. 1, pp. 420–428, Jan. 2006.

[5] A. Zapata *et al.*, "Next-generation 100-gigabit metro Ethernet (100 GbME) using multiwavelength optical rings," *J. Lightw. Technol.*, vol. 22, no. 11, pp. 2420–2434, Nov. 2004.

[6] G. Raybon, P. J. Winzer, and C. R. Doerr, "10 × 107-Gb/s electronically multiplexed and optically equalized NRZ transmission over 400 km," presented at the Optical Fiber Commun. Conf. (OFC) Postdeadline Papers, Anaheim, CA, 2006, Paper PDP32.

[7] M. Daikoku *et al.*, "100 Gb/s DQPSK transmission experiment without OTDM for 100 G Ethernet transport," presented at the Optical Fiber Commun. Conf. (OFC) Postdeadline Papers, Anaheim, CA, 2006, Paper PDP36.

[8] M. Cvijetic, *Coherent and Nonlinear Lightwave Communications*. Boston, MA: Artech House, 1996.

[9] H. Xiao-Yu *et al.*, "Efficient implementations of the sum–product algorithm for decoding of LDPC codes," in *Proc. IEEE Globecom*, Nov. 2001, vol. 2, pp. 1036–1036E.

[10] S. ten Brink, "Designing iterative decoding schemes with the extrinsic information transfer chart," *AEÜ Int. J. Electron. Comm.*, vol. 54, no. 6, pp. 389–398, Dec. 2000.

[11] J. Hou, P. H. Siegel, and L. B. Milstein, "Design of multi-input multi-output systems based on low-density parity-check codes," *IEEE Trans. Commun.*, vol. 53, no. 4, pp. 601–611, Apr. 2005.

[12] J. Tan and G. L. Stüber, "Analysis and design of symbol mappers for iteratively decoded BICM," *IEEE Trans. Wireless Comm.*, vol. 4, no. 2, pp. 662–672, Mar. 2005.

[13] I. Anderson, *Combinatorial Designs and Tournaments*. London, U.K.: Oxford Univ. Press, 1997.

[14] O. Milenkovic, I. B. Djordjevic, and B. Vasic, "Block-circulant low-density parity-check codes for optical communication systems," *IEEE J. Sel. Top. Quantum Electron.*, vol. 10, no. 2, pp. 294–299, Mar./Apr. 2004.

[15] J. L. Fan, "Array codes as low-density parity-check codes," in *Proc. 2nd Int. Symp. Turbo Codes Related Topics*, Brest, France, Sep. 2000, pp. 543–546.

[16] I. B. Djordjevic, H. G. Batshon, M. Cvijetic, L. Xu, and T. Wang, "PMD compensation by LDPC-coded turbo equalization," *IEEE Photon. Technol. Lett.*, vol. 19, no. 15, pp. 1163–1165, Aug. 1, 2007.

[17] J. G. Proakis, *Digital Communications*. Boston, MA: McGraw-Hill, 2001.

Ivan B. Djordjevic received the Ph.D. degree in electrical engineering from the University of Nis, Nis, Serbia, in 1999.

He was previously with the University of the West of England, Bristol, U.K.; the University of Bristol, Bristol; Tyco Telecommunications, Eatontown, NJ; the National Technical University of Athens, Athens, Greece; and Telecom Serbia, Nis. He is currently an Assistant Professor of electrical and computer engineering with the University of Arizona, Tucson. He is the author of more than 100 international publications. His current research interests include optical communication systems, error control coding, constrained coding, coded modulation, turbo equalization, and OFDM applications.

Milorad Cvijetic received the Ph.D. degree in electrical engineering from the University of Belgrade, Belgrade, Serbia, in 1984.

He was previously with Bell Northern Research (BNR, later NORTEL Technologies), Ottawa, ON, Canada. He has been with NEC Corporation of America, Herndon, VA, since 1997 and is currently the Vice President and the Chief Technology Strategist within the Optical Network Systems Division. He has taken part in numerous technical conferences and symposiums as a conference/session chairman, technical committee member, short course instructor, or invited speaker. He has published more than 70 technical papers and three books entitled *Digital Optical Communications, Coherent and Nonlinear Lightwave Communications*, and *Optical Transmission Systems Engineering*. He is also author or coauthor of seven U.S. patents.

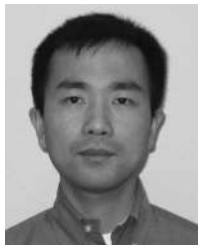

Lei Xu received the B.S. degree in geophysics from Peking University, Beijing, China, in 1997, the M.E. degree in electronic engineering from Tsinghua University, Beijing, in 2000, and the Ph.D. degree in electrical engineering from Princeton University, Princeton, NJ, in 2004.

Since 2004, he has been a Research Staff Member with NEC Laboratories America, Princeton. His current research interests include advanced modulation and coding schemes for optical communications, optical signal equalization and compensation, and innovative optical devices.

Ting Wang received the M.S. degree in electrical engineering from the City University of New York and the Ph.D. degree in electrical engineering from Nanjing University of Science and Technology, Nanjing, China.

Since 1991, he has been with NEC Laboratories America, Princeton, NJ, where he is currently the Department Head of optical networking research. He is the author or coauthor of approximately 70 publications and 30 U.S. patents.